Available online at www.sciencedirect.com
SCIENCE DIRECT®
Journal of Nuclear Materials 334 (2004) 47–57
journal of nuclear materials
www.elsevier.com/locate/jnucmat

Helium and xenon behaviour in irradiated Am-containing $MgAl_2O_4$ (reactor experiment EFTTRA-T4)

T.A.G. Wiss *, P.M.G. Damen, J-P. Hiernaut, C. Ronchi

European Commission, Joint Research Centre, Institute for Transuranium Elements, P.O. Box 2340, Karlsruhe D-76125, Germany

Received 13 October 2003; accepted 22 April 2004

Abstract

Magnesium aluminate spinel ($MgAl_2O_4$) containing ^{241}Am was irradiated for 358 days in the High Flux Reactor in Petten (NL) with the objective of effectively transmuting this highly radiotoxic actinide. The feasibility of the process was demonstrated; however, a major drawback was observed as material swelling, probably due to the large quantity of helium emitted from formed short-lived actinides. The behaviour of helium and of fission gas in the matrix was investigated by post-irradiation thermal annealing experiments in a Knudsen-cell. The observed gas release was related to the microstructure of the matrix investigated by scanning and transmission electron microscopy. Helium was found to be present in large pores, whereas the less mobile xenon was distributed partly in the same pores and partly in small intragranular bubbles. During post-irradiation thermal annealing, almost complete helium release took place abruptly at a rather high temperature (~1600 K), whilst only part of the xenon was released during this stage. The release of the remaining xenon was associated with a bulk thermal restructuring of the $MgAl_2O_4$ target at higher temperatures.

1. Introduction

Nuclear waste management has become a topic in the lively political and civilian debate on the sustainability of nuclear energy production. The main concern focuses on the issue of the high and long-lived radiotoxicity of spent fuel, whose major contributors are fission products like, e.g., ^{129}I and ^{99}Tc and actinides, like Pu, Am, Np and Cm.

To reduce the amount of this waste, 'partitioning and transmutation' (P&T) scenarios are studied in different international programmes [1]. Partitioning aims at separating minor actinides from spent fuel by using, for example, innovative liquid–liquid separation (e.g., the DIAMEX process [2]). Transmutation aims at converting the separated radiotoxic nuclides into stable or shorter-lived ones. This can be achieved in dedicated nuclear reactors by a combination of fission, neutron capture and radioactive decay processes [3]. In these irradiations, the actinides have to be incorporated in so-called 'inert matrix fuels' (IMF) that, contrary to usual fissile fuels, are effectively inert against neutron driven reactions.

The specific aspects of americium transmutation in a nuclear reactor have been studied as, e.g., by the EFTTRA [1] group. In the EFTTRA-T4 experiment, magnesium aluminate spinel, $MgAl_2O_4$, infiltrated with 10–12 wt% ^{241}Am, was irradiated in the High Flux Reactor (HFR) in Petten (NL) [4]. Table 1 summarises the main irradiation parameters as well as the geometrical

* Corresponding author. Tel.: +49-7247 951 447; fax: +49-7247 951 199.

E-mail addresses: wiss@itu.fzk.de (T.A.G. Wiss), hiernaut@itu.fzk.de (J.-P. Hiernaut), ronchi@itu.fzk.de (C. Ronchi).

[1] EFTTRA (Experimental Feasibility of Target for Transmutation) is a network of research organizations in France (EdF and CEA), Germany (JRC-ITU and FzK), and the Netherlands (JRC-IE and NRG).

0022-3115/$ - see front matter © 2004 Elsevier B.V. All rights reserved.
doi:10.1016/j.jnucmat.2004.04.347

Table 1
Main irradiation parameters of EFTTRA-T4

IMF composition	$MgAl_2O_4 + AmO_x$
Am-content ($g\,cm^{-3}$)	0.4
Irradiation time, EFPD	358.4
Irradiation duration (HFR cycles)	14
Neutron fluence ($\times 10^{25}$ m^{-2})	
$E > 0.1$ MeV	16.8
$E > 1$ MeV	8.04
Fission power, BOI/EOI ($W\,cm^{-3}$)	39/299[a]
Extent of transmutation	94.3
Extent of fission	27.9
Central temperature (K)	<1050
Al-structure temperature (K)	~670
Axial deformation of the column (%)	+4.5
Max. diametric deformation of the rod (%)	+6.7

[a] Recalculated by MCNP for the Am target.

changes of the inert matrix fuel stack after irradiation. The most notable observations at end-of-life (EOL) was the large swelling of the matrix (~18%) with formation of considerable porosity. Fig. 1 shows two optical micrographs of the EFTTRA-T4 material. In Fig. 1(a) the as-fabricated compound exhibits 2–3 μm sized Am-inclusions (bright spots) in a sintered matrix of ~4% porosity. Fig. 1(b) evidences the formation of a larger porosity after irradiation (~17%), more pronounced in some areas due to the initial higher local content in americium.

The rod was analysed after 358 days irradiation, when burn-up calculations predicted transmutation of 94% ^{241}Am, with formation of higher actinides from neutron capture; among them the strong alpha emitter ^{242}Cm ($T_{1/2} = 182.8$ days) and its daughter ^{238}Pu ($T_{1/2} = 87.74$ years). This resulted in the generation of large quantities of helium in the matrix, which eventually caused the formation of the observed high porosity. Prediction of the behaviour of helium in the matrix is of great importance since the balance between gas release and precipitation with formation of bubbles defines the IMF swelling rate and the eventual strength of the fuel/cladding mechanical interaction. These parameters are key indicators for the suitability of a given IMF for large scale application, especially in a 'once-through' scenario, where long irradiation times and high transmutation yields are required. In practice, two design options can be implemented based on whether or not the inert gas is mainly retained in the matrix or released in the smeared fuel rod porosity, which includes the fuel-cladding gap and the plenum. Fuel fabrication and rod design can therefore, be optimised if information on helium and fission gas release as a function of burn-up and irradiation temperature is available.

2. Experimental

Samples of a few tens of milligrams have been selected for SEM, TEM and Knudsen-cell effusion analysis. The radial position of the selected samples could be determined by SEM observations of the porosity whose size distribution was dependent on the initial Am-distribution. EPMA results show that the radial burn-up profile was rather flat with a slight increase toward the surface [5]. The analysed specimens were originating from a radial position close to $r/r_0 = 0.7$. Fragments of some tens of milligrams have been annealed in a Knudsen-cell (KC) at different temperatures and following different annealing programmes (at an average rate of, typically, 30 $K\,min^{-1}$). The species escaping from the sample were analysed on line by mass-spectrometry (a more detailed description of the apparatus can be found in Ref. [6]). The release profiles were evaluated as functions of time/temperature, and the different samples observed by scanning electron microscopy (SEM). The fuel was analysed by transmission electron microscopy (TEM) to investigate the defect microstructure after a storage time of approximately 4 years after irradiation

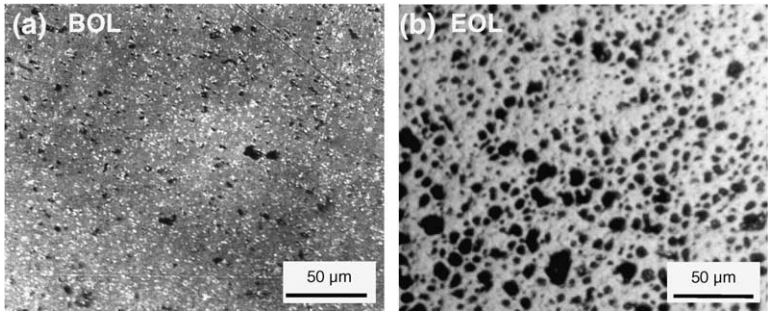

Fig. 1. Optical micrograph showing: (a) the as-fabricated sintered inert matrix with the dispersed 2–3 μm sized AmO_x inclusions (white spots); (b) the irradiated EFTTRA-T4 material exhibiting a porosity of on average 17%.

Table 2
Main isotope composition of the irradiated fuel at the time of the investigation (relevant inert gases are indicated in bold)

Isotope	Mass %	Atom %	Isotope	Mass %	Atom %	Isotope	Mass %	Atom %
^{4}**He**	**1.03E−01**	**5.72E−01**	^{107}Pd	6.08E−02	1.26E−02	^{234}U	1.25E−01	1.19E−02
^{16}O	4.09E+01	5.69E+01	^{108}Pd	4.63E−02	9.54E−03	^{235} U	2.88E−03	2.72E−04
^{24}Mg	1.48E+01	1.37E+01	^{131}**Xe**	**3.95E−02**	**6.70E−03**	^{237}Np	5.26E−03	4.94E−04
^{27}Al	3.34E+01	2.75E+01	^{132}**Xe**	**9.62E−02**	**1.62E−02**	^{238}Pu	4.16E+00	3.89E−01
^{94}Zr	4.04E−02	9.55E−03	^{133}Cs	8.22E−02	1.37E−02	^{239}Pu	7.11E−01	6.62E−02
^{95}Mo	4.20E−02	9.84E−03	^{134}**Xe**	**1.13E−01**	1.88E−02	^{240}Pu	2.15E−01	1.99E−02
^{96}Zr	4.95E−02	1.15E−02	^{136}**Xe**	**2.25E−01**	**3.67E−02**	^{24} Pu	1.36E−01	1.26E−02
^{97}Mo	5.44E−02	1.25E−02	^{137}Cs	1.06E−01	1.72E−02	^{24}Am	4.43E−01	4.09E−02
^{98}Mo	6.12E−02	1.39E−02	^{138}Ba	1.14E−01	1.83E−02	^{242}Pu	7.67E−01	7.05E−02
^{99}Tc	5.87E−02	1.32E−02	^{139}La	1.06E−01	1.70E−02	^{242m}Am	4.53E−03	4.16E−04
^{100}Mo	7.07E−02	1.57E−02	^{140}Ce	9.47E−02	1.50E−02	^{242}Cm	5.55E−03	5.10E−04
^{101}Ru	7.44E−02	1.64E−02	^{141}Pr	8.55E−02	1.35E−02	^{243}Am	5.71E−01	5.23E−02
^{102}Ru	8.89E−02	1.94E−02	^{142}Ce	8.56E−02	1.34E−02	^{243}Cm	9.33E−02	8.54E−03
^{103}Rh	1.19E−02	2.58E−03	^{143}Nd	5.07E−02	7.89E−03	^{244}Cm	5.35E−01	4.88E−02
^{104}Ru	8.97E−02	1.92E−02	^{144}Nd	8.43E−02	1.30E−02	^{245}Cm	4.69E−02	4.26E−03
^{105}Pd	6.28E−02	1.33E−02	^{145}Nd	5.06E−02	7.76E−03	^{246}Cm	1.56E−02	1.41E−03
^{106}Pd	8.47E−02	1.78E−02	^{146}Nd	5.51E−02	8.39E−03			

as well as after annealing at 1600 K. [2] The instrument used is a HITACHI STEM H700HST modified for handling of highly radioactive materials.

3. Results

During irradiation, thermocouples were placed on the outer part of the EFTTRA-T4 capsule. The outer temperature of the fuel rod was controlled by a helium cooling flow and maintained around 670 K, entailing a maximum centreline temperature of circa 1050 K.

Destructive post-irradiation examinations at EOL have been published in Ref. [7]. The isotopic composition of the irradiated material was evaluated from burn-up calculations by using the code OCTOPUS [8] from NRG, and neutron spectrum calculations obtained with the 3D Monte Carlo code MCNP-4B [9] in conjunction with the code FISPACT-4 [10]. From gas puncturing results and inventory calculations [11] the in-pile release was estimated around 20% for helium and 5% for fission gas. These values, accounting for the state of the fuel at EOL, have been corrected for the 4 years of storage preceding the reported investigations. In Table 2 the calculated concentrations of the main actinides and of other major fission/transmutation products are presented. The quantities of helium and xenon produced and retained in the matrix (indicated in appm) and the fraction released during irradiation are plotted in the bar-graph of Fig. 2. The helium produced during storage was calculated by using the Nuclides.net code [12]. It is assumed that the additional helium produced out-of-pile from alpha-emitters was frozen in the lattice. The percentage increase in helium concentration between EOL and the reported measurements is about 40% of the total inventory.

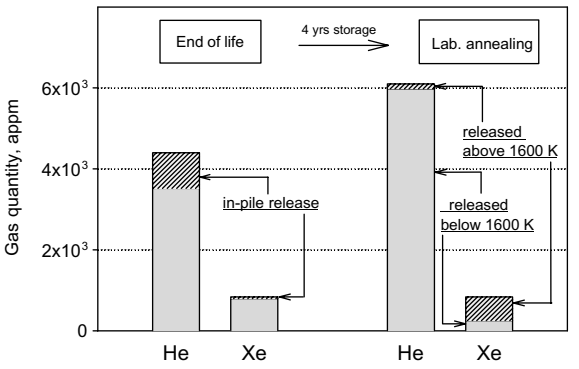

Fig. 2. Left-hand side bars: calculated quantity (indicated in appm) of helium and xenon produced during the irradiation of the EFTTRA-T4 target until end-of-life (EOL). The fraction of gas released was determined after puncturing of the irradiated capsule. Right-hand side bars: the additional He formed during storage from alpha-decaying actinides has been calculated from the inventory at EOL, using the Nuclides.net code [12]. The fraction of gas released during the Knudsen-cell experiment is indicated for the temperature (1600 K) at which the main He-release occurs.

[2] For this purpose, electron-transparent specimens have been prepared from small fragments of fuel by crushing them in ethanol and depositing a droplet of the obtained suspension on a TEM grid covered with a graphite film. For brittle ceramic materials the method produces particles with sufficiently representative transparent zones with no artefacts.

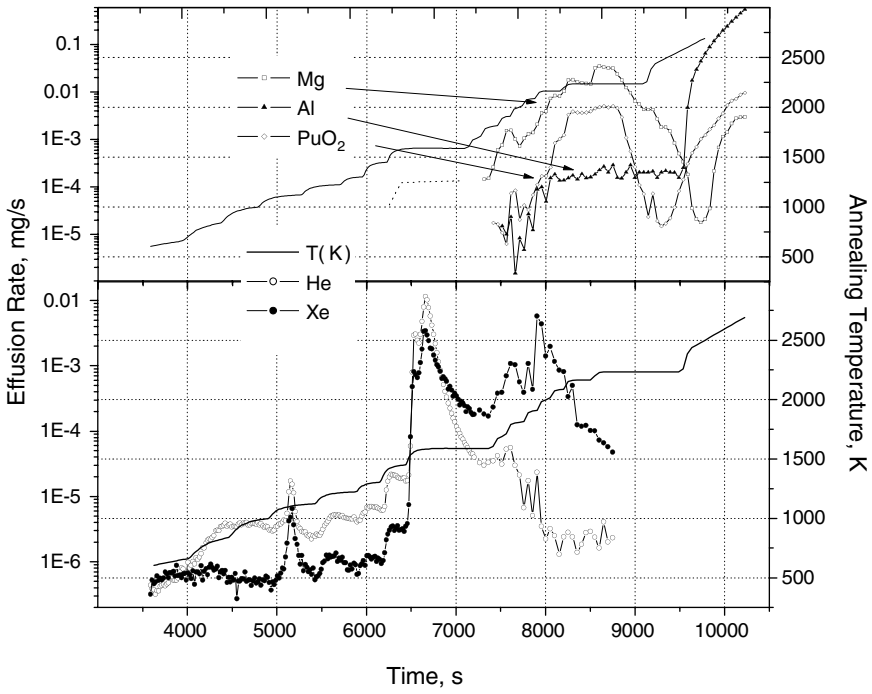

Fig. 3. Measured mass spectrometer signal of various fuel components. In the upper part of the graph are plotted the MS signals of the main components of the effusing vapour versus the annealing temperature. Bottom are plotted the results for the gases He and Xe.

The release–rate curves of He and Xe are shown in Fig. 3. Helium release starts at about 600 K, but the rate becomes significant only at 1550 K. Above this temperature it increases sharply, so that at 1600 K almost all helium is escaped within a few minutes. The picture is different for xenon. Though the fission gas appears to be

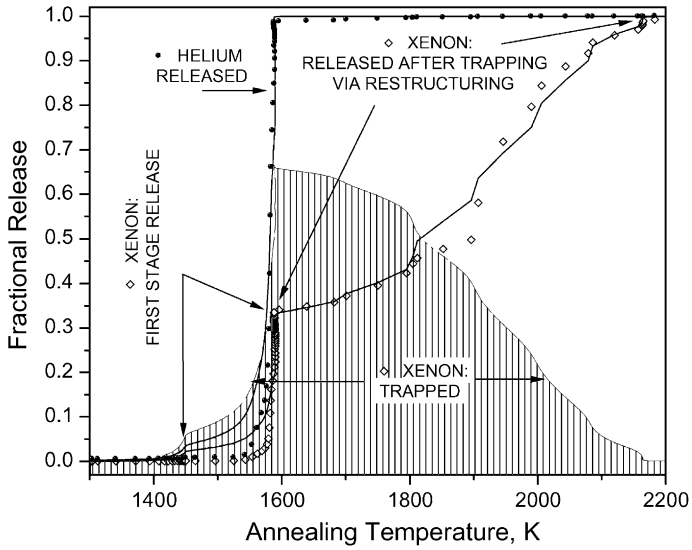

Fig. 4. Fractional release (normalised to the amount retained at EOL) of helium and xenon as a function of the thermal annealing temperature. The symbols represent the time integral of the effusion rate measured by MS, whilst the lines represent prediction of diffusion models. The dashed area represents the predicted fraction of xenon trapped in pores and subsequently release through matrix restructuring.

mobilised at the same temperatures as helium (see Fig. 4), the release rate peak around 1590 K involves only 35% of the xenon inventory. In fact, the remaining xenon is released in a second stage extending from 1600 K to approximately 1900 K.

Mass spectrometric measurements of the beam effusing from the sample indicate that magnesium starts subliming at an effective rate above 1600 K. Plutonium sublimation also increases above 2000 K at a dramatic rate, so that the sample eventually becomes markedly depleted in Mg and Pu (Fig. 3). This can be seen from the decrease of the MS signal of these elements by more than two orders of magnitude under constant temperature regime. Only above 2200 K does sublimation of aluminium take place, becoming predominant at temperatures above 2300 K.

SEM analysis of the samples was performed after different stages of the applied thermal annealing (Fig. 5). The ceramographic analysis of the fuel, described in more detail in Ref. [5], shows that the fabricated grains of 10 μm size have been reduced to small (~500 nm) subgrains after irradiation. Electron diffraction during TEM analysis shows that some regions of the matrix do not exhibit Bragg reflections; therefore, it can be conjectured that an amorphous state was created during reactor irradiation, and that some sort of re-crystallisation did slowly progress during the 4 years of storage. It is, however, noteworthy that after laboratory thermal annealing up to 1450 K no changes were observed on the surface morphology of the specimen, i.e., the large porosity and the matrix – constituted of small grains dispersed in a seemingly vitreous phase – are still visible in the micrographs (Fig. 5(a) and (b)). The first morphological changes of the sample surface were observed at 1600 K, i.e., just above the sharp gas release peak, where the grains have grown to a size range of the order of 1 μm, and clearly appear to be thermally etched, very likely due to Mg sublimation (Fig. 5(c)). At 2020 K the grain growth process is much more pronounced, producing grain sizes between 2 and 5 μm (Fig. 5(d)). At 2250 K two phases are unequivocally detected: the matrix, with grains of 5–20 μm size, and a phase enriched in plutonium and aluminium (Fig. 5(e)), consisting of rounded precipitates surrounding the matrix grains.

TEM investigations were performed before and after thermal annealing at 1600 K. The as-irradiated sample (labelled 'RT' in Fig. 6) clearly shows two phases; one (submicro)-crystalline phase of spinel with some fission product (FP) inclusions (Fig. 6(a)) and a Pu- and Al-rich phase containing gas bubbles of a few tens of

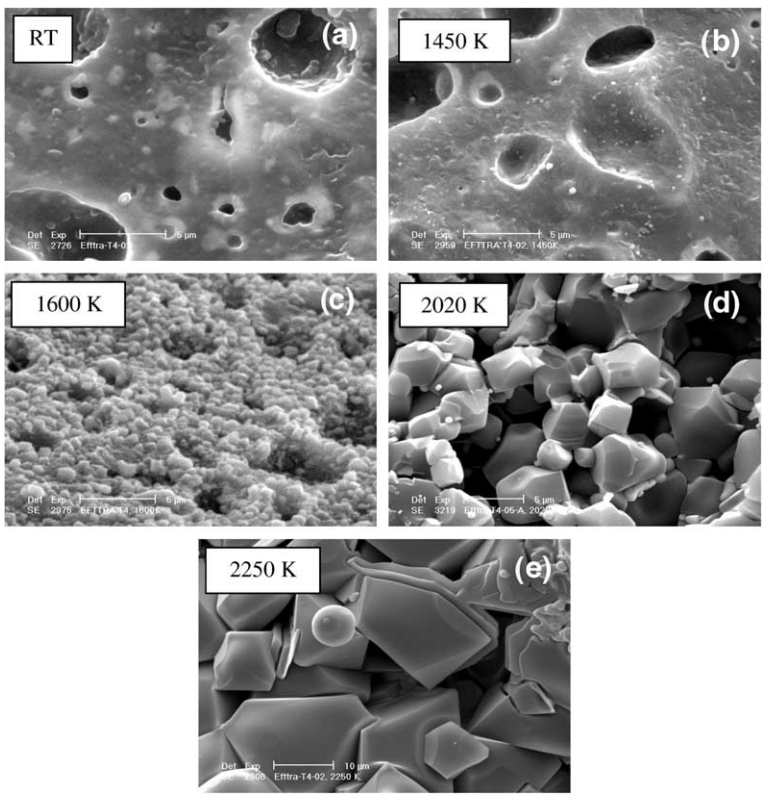

Fig. 5. SEM micrographs taken after different annealing stages showing the various material restructuring stages.

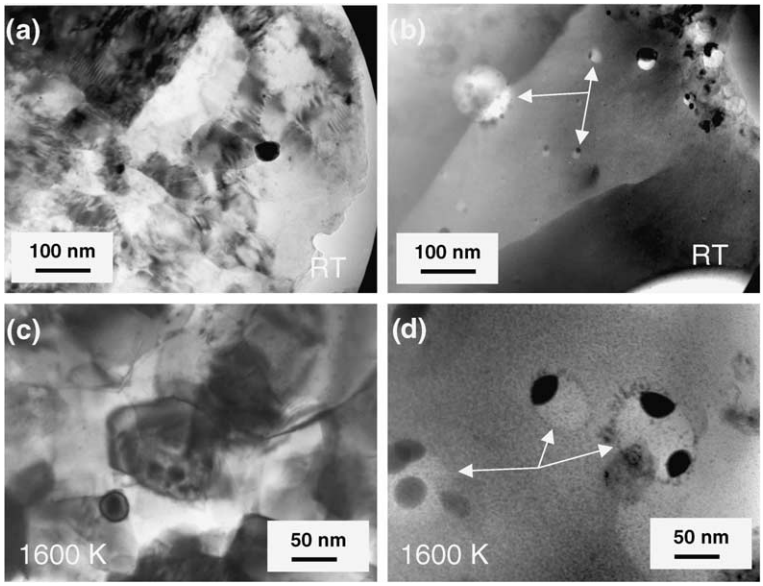

Fig. 6. Bright field TEM micrographs of an EFTTRA-T4 sample showing: (a) the matrix consisting of nano-sized grains with fission product precipitates; (b) the Pu-rich phase surrounding the pores contains gas bubbles of various sizes, often associated with fission product inclusions (arrows); (c) the matrix after annealing at 1600 K shows a pronounced change in the morphology of small grains; (d) presence of gas bubbles sizing around 50 nm (see arrow).

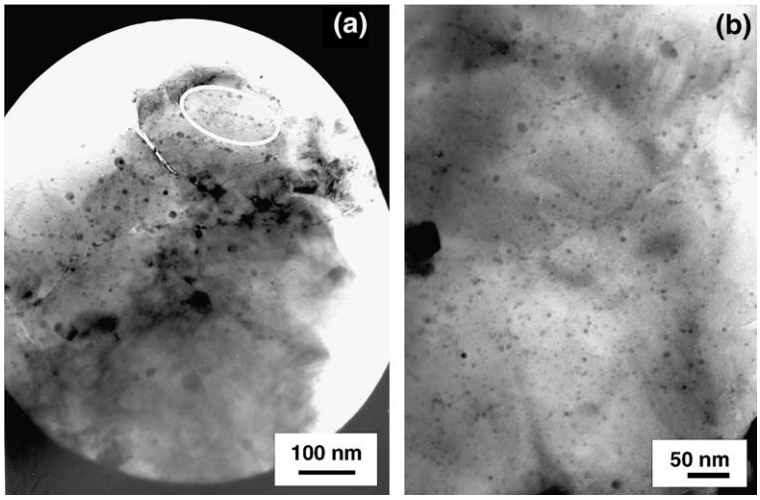

Fig. 7. Bright field TEM micrograph of the EFTTRA-T4 sample after annealing at 1600 K showing: (a) formation of small bubble strings in the matrix; (b) isolated nano-sized bubbles (bright circles), and numerous FP precipitates (black dots).

nanometres size, often associated with FP inclusions (Fig. 6(b)). From selected area electron diffraction patterns this latter phase appears to be quasi-amorphous, only weak traces of a crystal structure being occasionally observed. In the sample annealed at 1600 K the spinel matrix shows no radiation damage defects (Fig. 6(c)), but only scattered gas bubbles. In the (Pu, Al)-rich phase the gas bubbles are more numerous but similar in size to those observed in the EOL structure (Fig. 6(d)). Even after annealing at 1600 K, electron diffraction of the area of Fig. 6(d) (not shown here) reveals an amorphous background in the Pu-rich phase. Fig. 7 shows that bubbles are occasionally interconnected, forming short strings which may be ordered along possible gas perco-

lation paths, however, as shown in Fig. 7(b), most bubbles remain separate and randomly distributed in the matrix.

4. Discussion

The in-pile behaviour of the americium transmutation target is principally characterised by an exceedingly large swelling resulting from coarse porosity formation that is clearly manifested by the rod radial expansion at EOL, amounting to 4–5% of the initial diameter. The nature of the fuel/cladding mechanical interaction leading to such an expansion is still unknown. When referring to the state of the material at EOL, several parameters apparently affect gas bubble swelling. The microstructure is one of the prime factors that must be considered when interpreting release profiles from laboratory tests. In this section some comments on the features observed before and during thermal annealing are presented, together with a tentative analysis of the gas release measurements.

4.1. Structure and radiation damage

The as-irradiated material consists of a matrix of $MgAl_2O_4$ where a 1–2 μm thick, Pu-rich phase surrounds large pores (bright areas in Fig. 5(a)). This phase results from the americium infusion used in the fuel fabrication; its persistence at EOL corroborates the conjecture that the large pores have grown in pile *inside* the original Am-rich zones [5]. Furthermore, the pore interdistance (5–7 μm) is shorter than the range of the fission fragments. It is, therefore, plausible that the pores contain both helium and fission gas. Smaller gas bubbles were also observed, mainly dispersed in the Pu-rich phase surrounding the pores and often associated with metallic precipitates (see, e.g., Fig. 5(b) and (d)). In addition, Pu-rich inclusions (~100 nm) were found in the matrix by TEM investigations [5], but did not contain cavities.

The high concentration of inert gas, comparable to that created at fission burn-ups of the order of 100 GWd/t, might suggest an analogy with the RIM restructuring observed, for instance, in UO_2. Yet, distinctive features are observed in the EOL structure of spinel. The first one concerns the compactness of this material, which, despite ~20% swelling and in-pile thermal conditions, resulted in a high retention of the gas inventory (approximately 95% Xe and 80% He). The porosity was probably filled with gas at estimated pressures of the order of magnitude of 10 MPa. Very likely this closed type of porosity was formed and preserved during the irradiation and during the following thermal annealing as a result of the quasi-vitreous state of the damaged (ex-)spinel matrix, whose plasticity is evidenced by the absence of traces of micro-cracking around the perfectly rounded surfaces of the pores. [3] A further remarkable feature is the stability of this structure against thermal annealing up to temperatures far above the in-pile conditions.

The mechanisms of gas precipitation and their connection to radiation damage are apparently much more complex than in other, structurally more stable, materials. In particular, the probable amorphisation of the initial spinel in conjunction with the development of recrystallised sub-microscopic domains makes it difficult to identify the mechanisms of gas release, especially if these must be extrapolated from laboratory to in-pile conditions.

4.1.1. Helium

Previous investigations [13] have shown that helium implanted in spinel precipitates in bubbles if the gas concentration reaches approximately 1 at.%, and that blisters are formed on the ion bombarded surface [14].

Formation of He-bubbles in spinel was reported at an ion implantation dose of 1.8×10^{20} ions m^{-2} corresponding to ~8000 appm (60 keV, $^4He^+$) with a size of 0.9 nm at room temperature, and of 3.5 nm at 900 K [14].

Furthermore, helium release was studied by Knudsen-cell effusion [15] and by thermal helium desorption spectrometry (THDS) [15,16]. The peak temperature of the release rate – for annealing programmes comparable to those applied in this work – was shown to lie between 800 and 1600 K in polycrystalline spinel, depending on the implantation dose. The results of these studies show that release of implanted helium is delayed in polycrystals, as well as in cases where the implanted gas concentration is sufficiently high. This demonstrates that both sintered pores and vacancy clusters can act as efficient trapping sites for helium. The higher diffusion enthalpy measured in the latter case [15] may indicate a correspondingly large re-solution energy from highly pressurised trapping sites.

[3] When fission gas porosity is created with large sizes, the acting capillarity restraints are weak, and the effective isotropic stress exerted by a given amount of filling gas onto the surrounding matrix is inversely proportional to the fractional porosity. Under steady irradiation conditions and in the absence of gas release, the fuel swelling rate is constant, because the hydrostatic stress is effectively stationary as the result of the balance between the pore expansion and the linear increase of the gas inventory with time. Though this argument might appear very simplistic, this trend is confirmed qualitatively by the results of more realistic model calculations, also in cases where non-linear fuel creep rules are assumed. In reality, most ceramic fuels exhibit a constant swelling rate that, however, markedly decreases when the fission gas porosity exceed some critical venting threshold, whose magnitude is much lower than that observed in our spinel.

4.1.2. Xenon

The study of fission gas behaviour in spinel was investigated only in a few ion-implantation experiments, from which the following conclusions can be drawn: $MgAl_2O_4$ single-crystals irradiated with 340 keV Xe-ions to a dose of 10^{20} ions cm^{-2} at 100 K show formation of an amorphous layer. Xe-irradiated samples annealed and submitted to Rutherford backscattering channelling (RBSC) provide evidence that the material re-crystallises between 880 and 1120 K, but that xenon is effectively immobile below 1370 K and its presence does *not* affect re-crystallisation [17]. In a recent study [18] xenon release was measured from $MgAl_2O_4$ single-crystals irradiated under similar conditions (400 keV Xe-ions to a dose of 10^{20} ions m^{-2} at 100 K). The sample, rendered amorphous by Xe implantation, was subsequently implanted with 10^{19} He-ions m^{-2}. The release onset of xenon, occurring at 1050 K, was attributed to sweeping of gas atoms during re-crystallization of the amorphous spinel. Helium was released in an earlier stage, between 575 and 800 K.

The critical release temperature for helium in amorphous spinel implanted with helium is considerably lower than that observed in the EFTTRA-T4 material. By examining, however, the IMF microstructure it becomes evident that helium has first to escape from the Pu-rich phase surrounding the large pores before migrating through the spinel matrix. Since this microstructure does not exhibit any cracking around the pores, this process must be governed by gas- and/or self-diffusion. Furthermore, the microstructure of the spinel matrix, constituted of grains of some tens of nanometres, is unusual when compared to that available in the ion implantation experiments.

From the KC mass spectrometric measurements it can be seen that release of He and Xe is congruent with the calculated inventory (approximately 10:1) only during certain stages (see, e.g., the minor peak at 1150 K in Fig. 3). However, scrutiny of the fractional release curves of Fig. 4 reveals that the low temperature branch cannot be easily attributed to a thermally activated diffusion process. Helium and xenon are apparently escaping from common pockets, which become gradually vented as the temperature increases. These are probably pores located in the vicinity of the surface or that were near to critical percolation conditions.

When xenon is massively released above 1550 K and at higher temperatures, at which the matrix starts to sublime at a measurable rate, the concentration ratio of released He and Xe varies systematically, indicating a differentiation of the effective mobility of the two gases.

4.2. Release analysis

Diffusion models expressed by solutions of reaction rate equations, and successfully applied to solve a similar problem [19], have been used to interpret the sharp helium release peak between 1550 and 1600 K. However, in the present case the results were inconclusive, for data fitting by theoretical functions always gave uncertain solutions. This is comprehensible for a gas diffusion process occurring in a matrix that underwent thorough restructuring during measurements, i.e., irreversible collective processes dominated by internal energy changes of the defective lattice. [4] Nevertheless, all applied models indicate the occurrence of a gas sweeping/migration process activated by a high enthalpy (80–90 kcal $mole^{-1}$). The fitted pre-exponential factors of the rate equations (whose dimension is that of a frequency) are reported in Table 3. Their interpretation is not straightforward being dependent on the vibrational and configurational entropy changes of the system. If one interprets the gas migration as a correlated sequence of jumps of atoms vibrating at the Debye frequency (of approximately 10^{13} s^{-1}), the resulting gas migration entropy is of the order of magnitude of $-10R$ a value comparable to the entropies for lattice defect formation. This can indicate the occurrence of a collective (re)ordering process in the matrix structure. Though the argument may appear rather simplistic, it lends credit to the conclusion, reported in the preceding section, that the spinel, almost amorphous at EOL, after partial re-crystallisation during storage (perhaps due to electronic energy loss from the beta- and alpha-decaying fission products and actinides), underwent complete restructuring in the temperature interval 1550–1600 K. This explains the observation that almost no *intra* granular gas bubbles were present in the matrix at temperatures above this transition. Laboratory experiments on helium release from spinel, made amorphous by previous xenon implantation, have shown a similar behaviour, i.e., a sharp release of helium and subsequent release of xenon by grain boundary sweeping during re-crystallisation [18]. In our case, there is no doubt that all helium retained in the fuel was involved in the same, abrupt release stage, independently of its origin and its possible state at EOL and after storage. This implies a massive purging mechanism, driven by lattice reorganisation rather than by helium random diffusion. However, the most remarkable conclusion is that, once helium has reached grain boundaries or other extended defects, it is not permanently trapped, like xenon, in the coarse intergranular porosity, but almost immediately escapes to free surfaces. This was also observed in recent experiments carried out on irradiated $(U, Pu)O_2$, where,

[4] In view of the vagueness as to what activation enthalpy has to be used in the various terms of the reaction rate equation, the entropy change related to the diffusion process cannot be expressed with precision. However, even an estimate of ΔS, as it will be made below, can be indicative in checking experimental results. Unfortunately, in our case the scatter of the experimental data was too large for a quantitative analysis.

Table 3
Calculated gas migration parameters in the observed release stages

Gas	Release Stage I			Release Stage II		
	Enthalpy (kcal mole^{-1})	Pre-exp. (s^{-1})	Percentage of inventory	Enthalpy (kcal mole^{-1})	Pre-exp. (s^{-1})	Percentage of inventory
Helium	80–90	$4–9\times10^{8}$	~100	–	–	–
Xenon	80	$\sim6\times10^{7}$	30–40	82	6.1×10^{6}	70–60

contrary to our case, helium diffusion to trapping sites on grain boundaries was observed in a clearly identifiable stage. In spinel, trapping was apparently controlled by sweeping processes occurring during the bulk restructuring between 1550 and 1600 K and led to coincidental fast release.

The fraction of xenon still retained in the matrix at 1600 K after complete release of helium (Stage I), is subsequently released in a temperature range where the matrix starts subliming at a macroscopic rate (see Fig. 4), and this final release process (Stage II) is completed at temperatures at which PuO_2 is also subliming. This supports the hypothesis that this fraction of xenon is contained in closed pores (see micrograph in Fig. 5(d) and (e) after annealing at 2020 K).

In conclusion, release in Stage I is not effectively controlled by random diffusion of gas-in-solid, but by self-diffusion processes occurring in the bulk, biased by phenomenological forces due to matrix restructuring. Almost all helium and part of xenon are therefore dragged at a similar rate with the same activation enthalpy.

The difference in the pre-exponential factor of the effective diffusion coefficient of helium and xenon is likely due to the higher mobility of helium trapped on moving extended defects (dislocation networks, grain boundaries and sub-boundaries). Since, however, the gas migration enthalpy on these defects is low, this enhanced diffusion produces an increase of the apparent pre-exponential factor (more for helium than for xenon), without significantly affecting the apparent migration enthalpy of the gas released.

Contrary to the first stage, the analysis of the xenon release in Stage II (helium is practically absent in Stage II) brought positive results: the process could be sufficiently well described by a rapid trapping (in coincidence with the restructuring transition at 1550–1600 K) and a subsequent, thermally activated, diffusion process with an enthalpy of 80 ± 2 kcal mole^{-1}. Again, this is a relatively high energy for a gas atom diffusion process. If one considers that the pre-exponent of the gas diffusion coefficient in solid is normally $D_0 = 1$ cm^2 s^{-1}, the value of the pre-exponential coefficient of this stage (Table 3) is still too large for an atomic diffusion process and hence release, like in Stage I, should be rather attributed to a deeper matrix and pore restructuring governed by self-diffusion. In fact, the lower value of the pre-exponential factor in Stage II indicates that release is taking place in a more ordered structure than in Stage I. This explanation is supported by ceramographic observations before and after completion of Stage II (Fig. 5(c) and (d)), respectively) where the difference produced by restructuring are clearly visible.

In Fig. 4 are plotted the theoretical fitting curves of the fraction of xenon trapped and released. As mentioned above, the part of the curve at low temperature is rather inaccurate, whilst that at high temperature reproduces fairly well the experimental data. The theoretical curve for helium is also plotted in the same graph. In this case, the curve was fitted by an effective activation enthalpy of 79 kcal mole^{-1}. [5]

In Fig. 8, a general scheme summarising the observations and conclusions made on microstructure evolution, helium and xenon behaviour is represented.

4.3. Fabrication properties and in-pile performance of spinel IMF

The overall description of the gas behaviour and the analysis of the effects investigated in this paper do not take into account additional aspects of the fuel fabrication properties, which might be relevant for the in-pile performance of the examined IMF. The specific microstructure of the starting material did probably play a major role in the in-pile formation and growth of pores that mostly developed inside of the original 2–3 μm sized Am-inclusions, since their average size and inter-distance may define the characteristic release temperature of helium. In fact, the Pu-rich phase surrounding these pores was probably acting as a barrier for gas diffusion into the spinel matrix and may have played an important role in limiting gas release during the progressive, heavy radiation damage of the spinel lattice. Whether a more homogeneous initial distribution of the actinide phase can lead to a considerable amelioration of the in-pile performance of this material is still a matter of investigation.

[5] The fitting result is very uncertain as the numerical procedure can identify equally precise solutions in different energy ranges. The reported value is the most credible and, in its range, numerically stable (±5%).

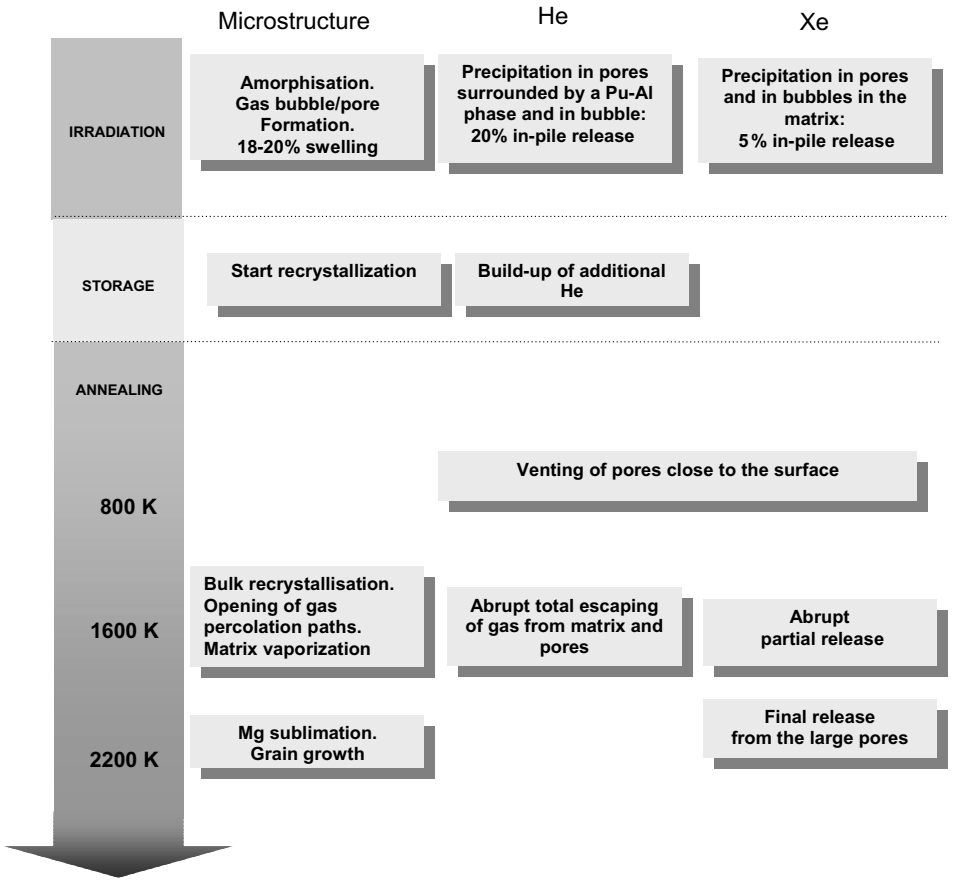

Fig. 8. Scheme of the He and Xe release mechanisms in the EFTTRA-T4 material associated to the microstructure changes produced by reactor irradiation and during laboratory annealing.

Finally, some considerations should be made regarding the thermochemical stability of spinel, which is limited by the relative high equilibrium vapour pressure of Mg(g). Analogously to MgO [20,21], the sublimation rate of spinel essentially depends on the environment oxygen potential.

At typical oxygen potentials levels buffered by cladding oxidation, and, a fortiori, under more reducing conditions, effective in-pile vaporisation processes must be expected in $MgAl_2O_4$, even at current IMF design temperatures. At temperatures attainable under power transient conditions or during reactor accidents one must expect massive evaporation/condensation processes in the fuel rod.

5. Conclusion

Spinel with 11.2 wt% ^{241}Am was successfully irradiated in the High Flux Reactor in Petten, and 94% americium transmutation was reached. However, the main drawback of this irradiation test was the very high gas swelling in the spinel target. The development of helium and fission gas filled porosity is causally related to the original microstructure (micro-dispersion of the actinide phase), which has affected the local evolution of radiation damage and gas precipitation. Helium was to a great extent trapped in pores formed within the original 2–3 μm sized Am-inclusions and in-pile release was low (20% for He and 5% for Xe).

When compared to ion-irradiated samples, gas release during post-irradiation thermal annealing occurs at higher temperatures in conjunction with a bulk restructuring of the heavily damaged spinel lattice. In the framework of such a mechanism, atomic diffusion of helium plays a secondary role compared with the strongly biased self-diffusion processes taking place in the matrix.

It has been shown that the $MgAl_2O_4$ spinel exhibits poor properties both from the thermochemical (strong preferential sublimation of Mg at moderate temperatures), and from the mechanical (weak restraining capacity of gas in bubbles) point of view.

In the development of new IMF targets, it becomes evident that both material and gas behaviour has to be accurately considered for the design of fuel rods. In this perspective, by considering aspects now known, there is no favourable argument to consider further this spinel as an inert matrix for actinide transmutation.

Acknowledgements

The authors are thankful to Dr Pijlgroms at NRG for burn-up calculations, and, at ITU, to F. Capone and J.-Y. Colle for their assistance in the Knudsen-cell measurements, and H. Thiele for the electron microscopy investigations.

References

[1] Actinide and fission product partitioning and transmutation, in: 6th Information Exchange Meeting, 2000, Madrid, Spain, EUR 19783 EN.
[2] C. Madic, P. Blanc, N. Condamines, P. Baron, L. Berthon, C. Nicol, C. Pozo, M. Lecomte, M. Philippe, M. Masson, C. Hecquet, M.J. Hudson, in: Fourth International Conference on Nuclear Fuel Reprocessing and Waste Management, RECOD'94, vol. 2, 1994, London, UK.
[3] R.J.M. Konings, Advanced fuel cycles for accelerator-driven systems: fuel fabrication and reprocessing, Report EUR 19928 EN, European Commission – JRC – ITU, 2001.
[4] A. Fernandez, K. Richter, J. Somers, J. Alloys Comp. 271 (1998) 616.
[5] T. Wiss, R.J.M. Konings, C.T. Walker, H. Thiele, J. Nucl. Mater. 320 (2003) 85.
[6] J.-P. Hiernaut, C. Ronchi, Report Euratom EUR 15154 EN, 1992.
[7] R.J.M. Konings, R. Conrad, G. Dassel, B. Pijlgroms, J. Somers, E. Toscano, The EFTTRA-T4 experiment on americium transmutation, Report EUR 19138 EN, 2000.
[8] J.L. Kloosterman, J.C. Kuijper, P.F.A. de Leege, The OCTOPUS burn-up and criticality code system, Report ECN-RX–96-032, Energieonderzoek Centrum Nederland, 1998.
[9] J.F. Briesmeister, in: MCNP, a general Monte Carlo Code for neutron and photon transport. Vers. 4a and 4b, Los Alamos National Laboratory, New Mexico, USA.
[10] R.A. Forrest, J.C. Sublet, FISPACT 4 User Manual, Easy Documentation series UKAEA FUS 287, Report UKAEA, 1995.
[11] B.J. Pijlgroms, Burn-up calculations for the EFTTRA T4 experiment, Report 21024/99.23088/P, Energieonderzoek Centrum Nederland, 1999.
[12] J. Magill, Nuclides.net, an Interactive Environment for Computations on Radionuclides and their Radiation, 2002, www.nuclides.net, Springer Verlag.
[13] N. Sasajima, T. Matsui, S. Furuno, T. Shiratori, K. Hojou, Nucl. Instrum. and Meth. B 166&167 (2000) 250.
[14] R. Fromknecht, J.-P. Hiernaut, H. Matzke, T. Wiss, Nucl. Instrum. and Meth. B 166&167 (2000) 263.
[15] E.A.C. Neeft, A. van Veen, R.P.C. Schram, F. Labohm, Prog. Nucl. Energy 38 (2001) 287.
[16] E.A.C. Neeft, R.P.C. Schram, A. van Veen, F. Labohm, A.V. Fedorov, Nucl. Instrum. and Meth. B 166&167 (2000) 238.
[17] I.V. Afanasyev-Charkin, R.M. Dickerson, D. Wayne Cooke, B.L. Bennett, V.T. Gritsyna, K.E. Sickafus, J. Nucl. Mater. 289 (2001) 110.
[18] P.M.G. Damen, A. van Veen, H. Matzke, H. Schut, J.A. Valdez, C.J. Wetteland, K. Sickafus, J. Nucl. Mater. 306 (2002) 180.
[19] C. Ronchi, J.-P. Hiernaut, J. Nucl. Mater. 325 (2003) 1.
[20] C. Ronchi, M. Sheindlin, J. Appl. Phys. 90 (7) (2001) 3325.
[21] T. Sasamoto, H. Hara, T. Sata, Bull. Chem. Soc. Jpn. 54 (1981) 3327.